2022

Effect Of Pressure Convection On The Energy Separation In Air Vortex Tube: Dimensional Analysis And Numerical Investigation

Junior Lagrandeur

Sergio Croquer

Sébastien Poncet

Effect of Pressure Work on the Energy Separation in Air Vortex Tube: Dimensional Analysis and Numerical Investigation

Junior LAGRANDEUR, Sergio CROQUER, Sébastien PONCET

Université de Sherbrooke, Department of Mechanical Engineering
Sherbrooke, Québec, Canada

Contact Information: Junior.Lagrandeur@USherbrooke.ca

ABSTRACT

In this work, a two-dimensional computational fluid dynamics (CFD) model of air vortex tube is used to investigate the effect of the pressure work from turbulence, which transfers energy in the direction of the strong outward pressure gradient generated by the swirling flow. The pressure work is considered by adding a term modelling it as an energy source in the CFD model. Prediction of the cold outlet temperature is good at high cold mass fractions, but some discrepancies remain at lower values. In addition, the inclusion of the pressure work inverts the radial static temperature profile near the inlet. Without it, the static temperature gets higher in the core, while it becomes lower with the additional term. To better understand where the pressure work is dominant inside the vortex tube and how it scales up with turbulence, the energy equation solved by ANSYS Fluent with the additional term is non-dimensionalized. The pressure work is proportional to the ratio of the pressure gradient divided by the local pressure ($\Delta P/P$). The pressure work, the heat transfer and the shear stress term all scale up with the turbulent viscosity ratio, meaning that turbulence level does not impact the relative importance of each of these terms. In the CFD model, the pressure work term is more important than the heat transfer and the shear stress term almost everywhere in the radial direction into the main tube. This highlights that it is important to model pressure work in future CFD simulations. However, the two-equation turbulence models do not predict the swirl decay adequately in the vortex tube. Consequently, the temperature gradient could be dominant in some additional areas near the hot end. New simulations may benefit from using advanced turbulence models which take into account both curvature and rotational effects in high swirling flows.

1. INTRODUCTION

The counterflow vortex tube, also called the Ranque-Hilsch vortex tube, is a device that splits a stream of compressed gas into two streams with different temperatures. To achieve this, the high-pressure gas is injected tangentially to form a strong swirling flow inside the tube. As shown in Figure 1, the inlet Mach number is high, meaning the flow is compressible. After the inlet, part of the flow goes to the other end of the tube and leaves through the hot outlet. Another part of the gas creates a reverse flow in the core, a form of vortex breakdown. This flow goes out through an opening in the core of the tube located near the inlet and named the cold outlet. The fraction of the inlet mass flow that goes through the cold outlet is called the cold mass fraction (μ_c).

The energy separation mechanism is hard to explain. Xue et al. (2010) provided a critical review of different explanations for the energy separation mechanism. They concluded that the temperature drop can be the result of sudden expansion near the inlet, but no mechanism explains the energy transfer between the core and the periphery. Lagrandeur, Poncet, and Sorin (2019) reviewed predictive models and highlighted that heat transfer alone cannot explain the energy transfer given that some authors (Gao, 2005; Khait et al., 2014) reported that the static temperature in the core is lower than the temperature at the periphery.

Some authors used Computational Fluid Dynamics (CFD) to investigate the energy separation process. Aljuwayhel et al. (2005) performed two-dimensional (2D) CFD calculations with the standard $k-\varepsilon$ and the RNG $k-\varepsilon$ turbulence models to define three areas: the cold flow region, the hot flow region and a recirculation region. They demonstrated that the tangential shear stress is the main mechanism of energy transfer from the cold flow region to the hot flow region. Behera et al. (2008) obtained similar results with a 60^o sector using the RNG $k-\varepsilon$ model. Bej and Sinhamahapatra (2016) used a 2D model with the standard $k-\varepsilon$ to analyze the energy transfer at different axial and radial locations, but without defining the boundary between the hot and the cold flows. They found that the tangential shear work is

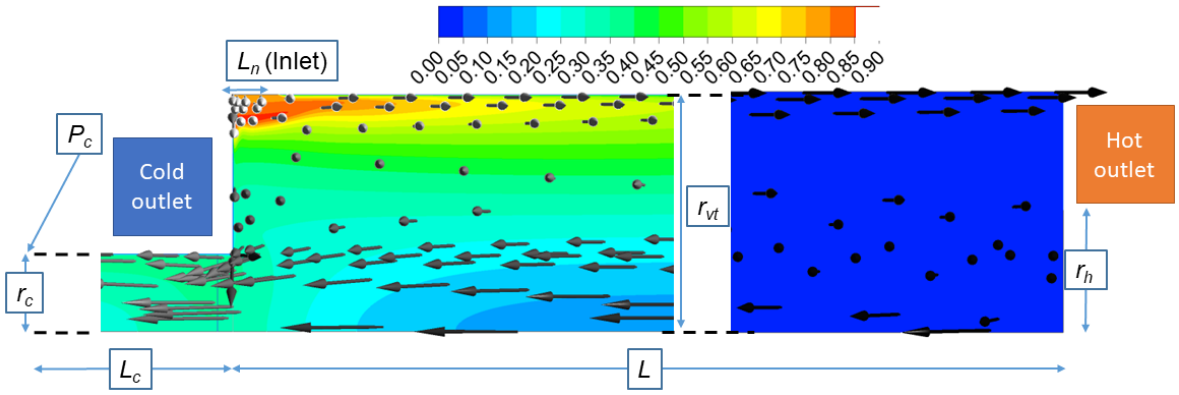

Figure 1: Example of Mach number contours in the vortex tube with the flow pattern and main dimensions.

important, but that heat transfer may degrade the performance near the inlet. Maximum temperature separation occurs in the first half of the tube (length L_{vt}), but not really close to the inlet. Dutta et al. (2021) repeated this analysis on a 60^o sector to compare the counterflow and the uniflow vortex tube. They confirmed that the tangential shear stress is dominant, but also that heat transfer and axial shear stress are detrimental in the energy separation process.

Dyck and Straatman (2018) also used a 2D model with the standard $k-\varepsilon$ closure to quantify the impact on the energy transfer of different terms for different cold mass fractions. Their analysis replicated the vortex tube used by Skye et al. (2006). They found that the tangential shear stress is the main mechanism producing positive radial energy transfer. However, they noticed that the CFD model underpredicted the energy separation, which was also highlighted by Chen et al. (2018). Even using large eddy simulation on the same geometry, this discrepancy remained (Farouk & Farouk, 2007).

An explanation for the missing energy transfer may be obtained using analytical models. Based on the potential laminar flow theory, Shtern and Borissov (2010) showed that the pressure convection, which is the inner product of velocity and of the pressure gradient, counterbalances the temperature convection for a non-zero radial velocity flow in a strong radial pressure gradient. If the heat conduction is small, the radial temperature profile is isentropic, as confirmed by Tyutyuma (2016).

For turbulent flows, Deissler and Perlmutter (1960) obtained the same isentropic profile by introducing a term in the energy equation that is a product of the eddy diffusivity (ε) and the derivative of pressure in the radial direction. Cockerill (1998) also included a term which considers the pressure gradient in a turbulent rotating flow field, and found this term is fundamental to explain the energy separation process. In this case, the pressure gradient could transfer energy from the core to the periphery using the radial fluctuations instead of the mean negative radial velocity. This energy exchange process is similar to a heat pump (Kolmes et al., 2017).

Khait et al. (2014) and Kobiela et al. (2018) noticed that the pressure gradient term is neglected in typical calculations using Reynolds-Averaged Navier-Stokes equations because turbulent mixing is dominant in most practical turbulent flows. They both proposed a new algebraic source term in the energy equation to model the pressure convection effect. The energy source proposed by Khait et al. (2014) writes:

$$S_{kh} = -\nabla \cdot \left(\lambda_{eff} \frac{\gamma - 1}{\gamma} \frac{T}{P} \nabla P \right), \tag{1}$$

with S_{kh} the additional energy source term, γ the specific heat ratio, T the static temperature and P the static pressure. λ_{eff} is the effective thermal conductivity, which is the sum of the gas molecular thermal conductivity and of the turbulent thermal conductivity calculated from the turbulence model. S_{kh} is almost identical to the term presented by Cockerill (1998). The term proposed by Kobiela et al. (2018) is more general, but it reverts to the same expression for the limiting case of a perfect gas with turbulent particles moving adiabatically in the radial direction. Khait et al. (2014) created a full 3D model of vortex tube using a density-based solver with the standard $k-\varepsilon$ model. A good agreement with experimental results was obtained only when S_{kh} is included.

Table 1: Main dimensions in mm of the vortex tube as defined in Fig. 1.

Vortex tube radius	r_{vt}	12.7
Vortex tube length	L	693
Cold tube radius	r_c	4.125
Cold tube length	L_c	50.8
Inlet width	L_n	2.54
Radius difference for the annular hot outlet	r_h	6.35

In this work, the relative effect of the pressure work, modeled using S_{kh}, will be analyzed using both dimensional analysis and a 2D CFD model of the vortex tube tested by Camiré (1995). First, the energy equation with the additional source term will be normalized to identify scaling parameters for the energy exchange mechanisms. Then, these parameters will be compared using the numerical model to identify which energy transfer mode is dominant in each part of the tube.

2. MATERIAL AND METHODS

2.1 Numerical Methods

A 2D axisymmetric numerical model of the vortex tube developed by Camiré (1995) is simulated using ANSYS Fluent 2020 R2. Dimensions are provided in Table 1 and their localization is shown in Figure 1.

Lagrandeur et al. (2021) validated the model by comparing the cold outlet temperature and the hot outlet pressure with experimental values. The optimal simulation parameters have also been identified. In this work, the implicit density-based solver with the Roe-FDS flux is used with a Third-Order MUSCL scheme for the spatial discretization. Air is considered as the working fluid with variable thermodynamic properties calculated using the expressions suggested in Ouadha et al. (2013). Density is computed using the ideal gas law. The Favre-Averaged Navier-Stokes equations are closed using the $k-\omega$ SST turbulence model, which is a low-Reynolds number formulation by nature. Gradients are evaluated by the least squares cell-based approach.

The structured mesh with 637,551 elements was generated using ICEM and guarantees $y^+<5$ everywhere, a prerequisite for a low-Reynolds number formulation.

Regarding the boundary conditions, experimental values are used at both outlets. The hot outlet pressure is a mean value. For the cold outlet, the pressure is measured at the wall in the experiments. The radial pressure equilibrium option is used for this boundary to model the pressure increase in the radial direction induced by swirl. A velocity inlet condition is imposed. The tangential velocity is initialized using the value computed from an analytical model (Lagrandeur, Poncet, Sorin, & Khennich, 2019), but a radial velocity is also necessary to obtain the inlet mass flow rate in the axisymetric inlet. Iterations are done on these velocities to match the total pressure and the inlet mass flow rate from the experiments. The turbulence level at the inlet has been changed from 2% to 10% without any significant influence. The no-slip condition is used for all walls. The vortex tube wall is made of glass and so has been considered as smooth. However typical surface roughness values are implemented for surfaces made of other materials.

2.2 Normalization of the Energy Equation

Within ANSYS Fluent, the steady-state energy equation neglects diffusion of species and so writes (ANSYS, 2022):

$$\nabla \cdot \left[\rho \vec{v}\left(h + V^2/2\right)\right] = \nabla \cdot \left(\lambda_{eff} \nabla T\right) + \nabla \cdot \left(\bar{\bar{\tau}}_{eff} \cdot \vec{v}\right), \tag{2}$$

with ρ the static density, V the velocity magnitude, $\vec{v}$ the velocity vector, $h = e + p/\rho$ the specific static enthalpy, e the internal energy and $\bar{\bar{\tau}}_{eff}$ the effective viscous stress tensor. In this equation, the pressure convection is included as a part of the enthalpy on the left hand-side. All quantities are mean values of the turbulent flow except when indicated.

Lamberts (2018) redevelopped the Favre-averaged Navier-Stokes equations. He obtained the same equations under the following assumptions:

1. the turbulence kinetic energy is neglected in the calculation of the total energy;
2. molecular diffusion and turbulent transport of kinetic energy are neglected;

3. the pressure gradient source term $\overline{\vec{v}'' \nabla P}$ is neglected, with $\vec{v}''$ the vector of velocity fluctuations.

These assumptions are implicitly used to obtain the energy equation within ANSYS Fluent. The term neglected in the third hypothesis represents the energy exchange by turbulent eddies across a pressure gradient. This term is positive, meaning that energy is flowing in the same direction as the pressure gradient. For vortex tube, because the pressure gradient is strong in the radial direction, an energy flux from the core to the periphery is obtained. As explained by Wilcox (1998), the pressure gradient term vanishes in incompressible flows with zero density fluctuation. All pressure effects (pressure diffusion, dilatation and work) are generally neglected because there is no generally accepted model for these, there is a lack of experimental results to validate the few existing models and because the pressure gradient is small for common flows.

With the addition of S_{kh} from Equation (1), assuming axisymmetry and considering that $h = C_p T$ for a perfect gas, with C_p the specific heat at constant pressure, Equation (2) could be rewritten as:

$$\nabla \cdot \left[\overbrace{\rho \vec{v} \left(C_p T + V^2/2 \right)}^{\#1} - \overbrace{\lambda_{eff} \nabla T}^{\#2} - \overbrace{\bar{\bar{\tau}}_{eff} \vec{v}}^{\#3} + \overbrace{\lambda_{eff} \frac{\gamma - 1}{\gamma} \frac{T}{P} \nabla P}^{\#4} \right] = 0. \tag{3}$$

In Equation (3), the first term represents the transport of enthalpy and kinetic energy by the bulk flow, the second term is the heat flux modelled using the Fourier's law, the third term is the work done by the shear stress and the fourth term is the work done by the pressure gradient.

The turbulent viscosity (μ_t) is far greater than the molecular value in vortex tubes (Lagrandeur et al., 2021). Consequently, $\mu_{eff} \approx \mu_t$ and $\lambda_{eff} \approx \lambda_t$. λ_{eff} and τ_{eff} could be rewritten as:

$$\lambda_{eff} = \frac{\mu_t C_p}{\mathrm{Pr}_t}, \tag{4}$$

$$\tau_{eff} = \approx \mu_t \left[\nabla \vec{v} + \nabla \vec{v}^T - \frac{2}{3} tr \left(\nabla \vec{v} \right) \bar{\bar{I}} \right] = \mu_t \bar{\bar{B}}, \tag{5}$$

with Pr_t the turbulent Prandlt number, $\bar{\bar{I}}$ the identity tensor and $\bar{\bar{B}}$ the velocity tensor. Replacing λ_{eff} and τ_{eff} and dividing each term by the specific perfect gas constant R to normalize C_p in Equation (2) give:

$$\nabla \cdot \left[\overbrace{\frac{\gamma}{\gamma - 1} \rho \vec{v} \left(T + \frac{V^2}{2 C_p} \right)}^{\#1} - \overbrace{\frac{\mu_t}{\mathrm{Pr}_t} \frac{\gamma}{\gamma - 1} \nabla T}^{\#2} - \overbrace{\frac{\mu_t B \vec{v}}{R}}^{\#3} + \overbrace{\frac{\mu_t}{\mathrm{Pr}_t} \frac{T}{P} \nabla P}^{\#4} \right] = 0. \tag{6}$$

Equation (6) could be normalized using the vortex tube diameter (D_{vt}) as the characteristic length, the forced vortex angular velocity at the inlet ($\omega_{a,in}$) for the characteristic time, the total density at the inlet (ρ_{0in}) for the mass and the total temperature at the inlet (T_{0in}) for the temperature. Equation (6) is rewritten as:

$$\nabla^* \cdot \left[\overbrace{\mathrm{Pr}_t \frac{\gamma}{\gamma - 1} \rho^* \frac{\vec{v}}{\omega_{a,in} D_{vt}} \left(T^* + \frac{\mathrm{Ec}}{2} \right)}^{\#1} - \overbrace{\frac{\mu_t}{\rho_{0in} D_{vt}^2 \omega_{a,in}} \frac{\gamma}{\gamma - 1} \frac{\nabla^* T}{T_{0in}}}^{\#2} - \overbrace{\mathrm{Pr}_t \frac{\mu_t}{\rho_{0in} D_{vt}^2 \omega_{a,in}} \frac{D_{vt} B \vec{v}}{R T_{0in}}}^{\#3} + \overbrace{\frac{\mu_t}{\rho_{0in} D_{vt}^2 \omega_a} T^* \frac{\nabla^* P}{P}}^{\#4} \right] = 0, \tag{7}$$

with $\nabla^* = D_{vt} \nabla$ the dimensionless gradient and divergence operator, $\rho^* = \rho \rho_{0in}^{-1}$ the dimensionless density, $T^* = T T_{0in}^{-1}$ the dimensionless temperature, Ec is analog to the Eckert number $\mathrm{Ec} = V^2 C_p^{-1} T_{0in}^{-1}$. One could note a term similar

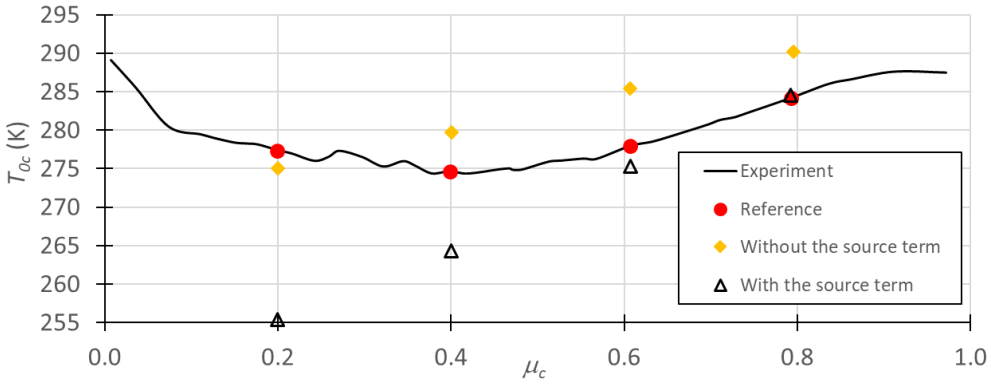

Figure 2: CFD results with and without the source term from Equation 1 compared with the experimental results of Camiré (1995) for an inlet pressure of 239 kPa.

to the Reynolds number in terms # 2 to # 4. The Reynolds number could be obtained by introducing the molecular viscosity μ and the inlet velocity $v_{in} = 0.5\omega_a D_{vt}$. In addition, the speed of sound ($c = \sqrt{\gamma RT}$) could be obtained in term #3 by introducing γ and T. Since the flow is compressible, the speed of sound could also be introduced in term #1 to express velocity using the Mach number. After some rearrangement, the final dimensionless form of the energy equation is:

$$\nabla^* \cdot \left[\overbrace{\mathrm{Pr}_t \mathrm{Re}_D \frac{\rho^*}{\mu_t^*} \frac{\vec{\mathrm{Ma}}}{\mathrm{Ma}_{in}} c^* \left(1 + \frac{\mathrm{Ec}}{2T^*}\right)}^{\#1} - \overbrace{\frac{\nabla^* T}{T}}^{\#2} - \overbrace{(\gamma - 1)\,\mathrm{Pr}_t \frac{D_{vt} B}{c} \vec{\mathrm{Ma}}}^{\#3} + \overbrace{\frac{\gamma - 1}{\gamma} \frac{\nabla^* P}{P}}^{\#4} \right] = 0, \tag{8}$$

with $\mathrm{Re}_D = \rho_{0in} u_0 D_{vt} \mu^{-1}$ the Reynolds number based on the diameter and on the total density at the inlet, $\mu_t^* = \mu_t \mu^{-1}$ the turbulent viscosity ratio, c^* the ratio of the local speed of sound to the speed of sound at the inlet (c_{0in}), $\vec{\mathrm{Ma}}$ the velocity vector express in terms of Mach number, Ma_{in} the inlet Mach number.

Equation (8) is similar to the dimensionless form of the energy equation provided by Stephan et al. (1984) using laminar flow energy equation and by Kaufmann (2022) for the enthalpy balance in the boundary layer of the vortex tube. However, this equation is different because it includes term # 4, which expresses the pressure gradient, and because it uses the speed of sound to obtain the Mach number, which is a better method to normalize the velocity for compressible flows. In addition, because λ_t is calculated using the turbulent viscosity, the Fourier number found by Kaufmann (2022) does not appear in this equation.

From Equation 8, one could observe that terms #2 to #4 do not depend on turbulent quantities. This means that their relative importance does not depend on the turbulent viscosity predicted by the turbulence model. They depend only on mean flow variables and their spatial derivatives. This may partly explain why the temperature separation predicted by the standard $k - \varepsilon$ is similar to the one predicted by the $k - \omega$ SST model in Lagrandeur et al. (2021) even if μ_t^* is much higher for the $k - \varepsilon$ model.

In the next section, the relative magnitude of term #4 will be compared to the others using CFD results.

3. RESULTS AND DISCUSSION

3.1 Prediction of the cold outlet temperature with the source term

Figure 2 shows the impact of the additional source term on the prediction of the CFD model. One could observe that, without the source term, the CFD model underpredicts the temperature drop in the vortex tube. With the pressure work terms, predictions are really good at high cold mass fractions. However, at low cold mass fractions, the total cold outlet temperature (T_{0c}) continues to drop as a linear function of the cold mass fraction. The same behaviour is observed without the source term. In this case, results from the simulation without the source term are closer to

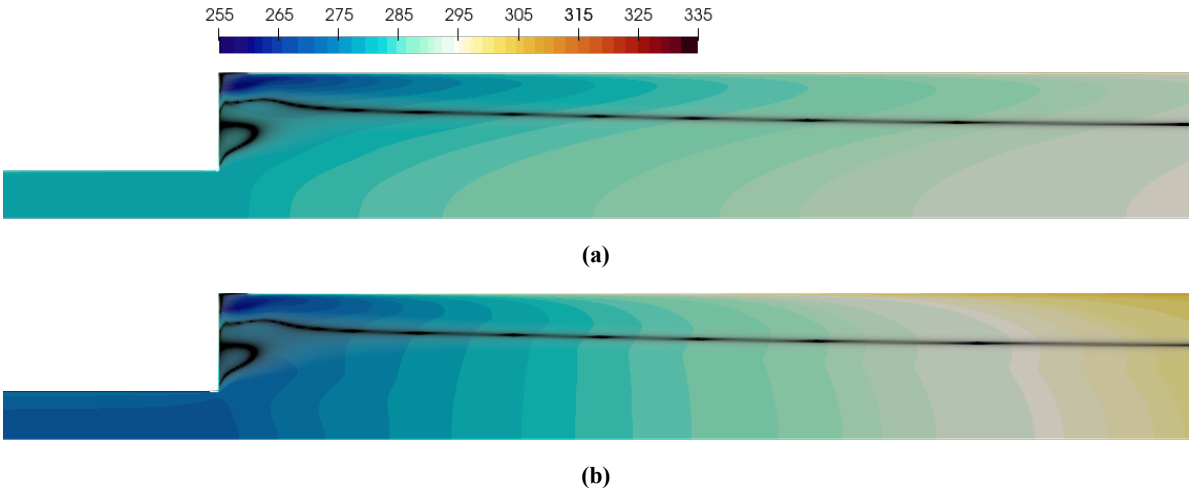

Figure 3: Static temperature contours (in K) near the inlet (a) without the pressure convection source term and (b) with the source term for P_{0in}=239 kPa and μ_c=0.6. The black line delimits the flow reversal zone.

experimental results, but the shape of the curve is not improved. In fact, the increase in the cold outlet temperature at low cold mass fractions may be caused by the occurrence of a vortex breakdown in the cold tube when the axial momentum is low. Flow reversal in the cold tube at low cold mass fraction has been confirmed experimentally (Yusof et al., 2015) and numerically (Lagrandeur et al., 2021). Yusof et al. (2015) demonstrated that the lower cold outlet temperature is obtained just before the beginning of the flow reversal in the cold tube.

Figure 3 illustrates the effect of the additional source term on the static temperature profile. The flow reversal zone, which is defined here as the location where the axial velocity approaches zero, is also shown on the figure. Without the source term, the static temperature in the core is always higher than at the periphery, meaning the heat transfer by conduction is from the core to the periphery. However, the source term is necessary to obtain the reverse static temperature profile measured by Gao (2005).

3.2 Comparison of the pressure energy source with other modes of energy transfer

In this section, the pressure convection term S_{kh} is compared in magnitude with the other terms in Equation (8). Figure 4a shows the ratio between the pressure convection (term # 4) and the turbulent temperature conduction (term # 2) in the radial direction. One can observe that the pressure gradient term is one order of magnitude higher than the temperature gradient term across the flow reversal line, meaning that energy flows outward due to the work done by the pressure gradient. Although not shown here, pressure convection remains as the dominant term across the flow reversal line up to the detwister near the hot end. Temperature convection is dominant in the boundary layer where the swirl is almost zero. Similar results are obtained for the seven other simulations for different P_{0in} and μ_c values.

Figure 4b displays the ratio between the energy transfer by pressure convection and the energy transfer by shear stress in the radial direction. Once again, the pressure convection term is dominant by one order of magnitude. It is true for all the vortex tube lengthes and for all others investigated conditions. Again, the shear stress is dominant only in the boundary layer.

Figure 4 highlights the importance of the pressure work term in the vortex tube core, where the pressure gradient is strong enough to make it the dominant energy source term. However, the pressure gradient is strongly dependent on the tangential velocity profile. The $k-\omega$ SST turbulence model used here predicts a forced vortex velocity profile along all the length of the vortex tube, which is different from measured velocity profiles (Lagrandeur et al., 2021). It would be interesting to repeat this analysis with a more complex turbulence model that could accurately predict the tangential velocity profile.

Finally, all figures show the separation line with zero axial velocity, but it is necessary to determine the direction of the flow in the radial direction to establish if the flow goes inward. The radial velocity is negative across the flow reversal line in most of the vortex tube at all inlet pressures, and cold mass fractions investigated. Near the inlet, a

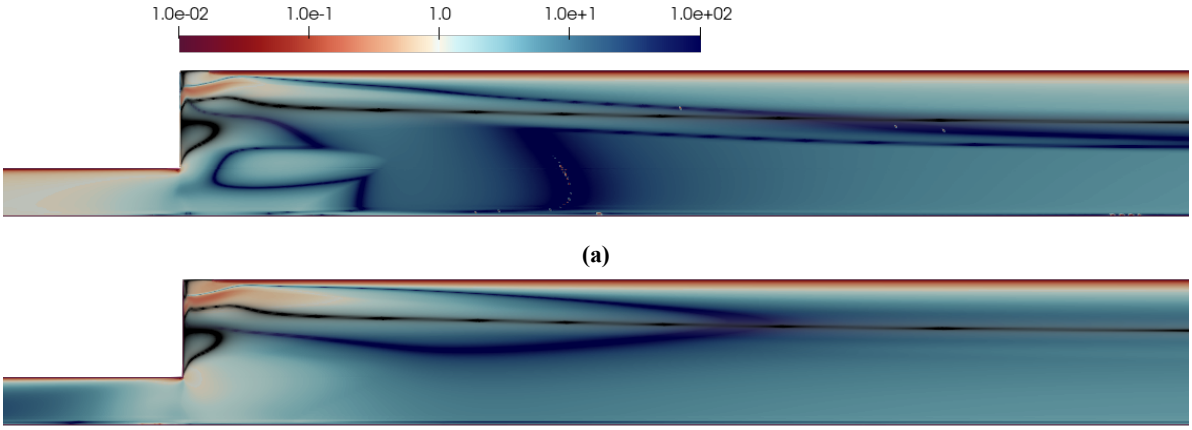

Figure 4: Ratios in the radial direction of (a) terms # 4 and # 2 from Eq. (8) and of (b) terms # 4 and # 3 for P_{0in}=239 kPa and μ_c=0.6. The black line delimits the flow reversal zone.

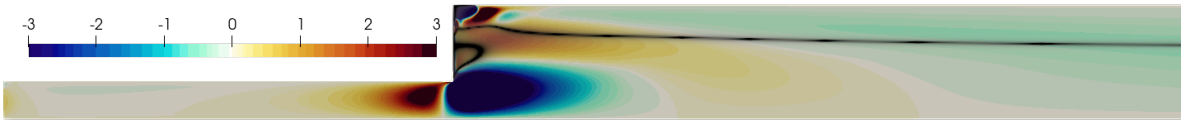

Figure 5: Radial velocity (in m· s^{-1}) near the inlet and in the cold outlet of the vortex tube for P_{0in}=239 kPa and μ_c=0.6. The black line delimits the flow reversal zone.

zone with positive radial velocity is observed as shown in Figure 5. One could observe that a recirculation zone with positive radial velocity is found across the flow reversal line near the inlet. This positive radial velocity brings fluid with low total temperature over the flow reversal line as shown in Figure 6. This could reduce the energy separation by cancelling out the energy transfer from the pressure gradient near the inlet as proposed by Behera et al. (2005). However, deeper investigation is necessary to confirm this statement.

Even if it is not shown here, this recirculation zone is similar in shape for different inlet pressures. However, it is observed that the recirculation zone enlarges when the cold mass fraction is reduced. This is surprising since some authors stated that the reciculation zone is related to an undersized cold outlet (Behera et al., 2005). Even if a larger cold outlet has not been investigated here, it was expected that the recirculation zone would become larger when the mass flow through the cold outlet increases, but the opposite behaviour is observed here.

4. CONCLUSION

Since its invention, the energy transfer mechanism in the Ranque-Hilsch vortex tube has been a subject of debate. In this article, the effect of the turbulent pressure work was investigated. This term in the energy equation is proportional to the pressure gradient and only appears in the Favre-Averaged Navier-Stokes equations for compressible fluids. The effect of this term has been studied by adding a source term as proposed by Khait et al. (2014) to a 2D CFD model using Fluent. Adding this term improved the prediction of the cold outlet temperature. In addition, it inverses the static

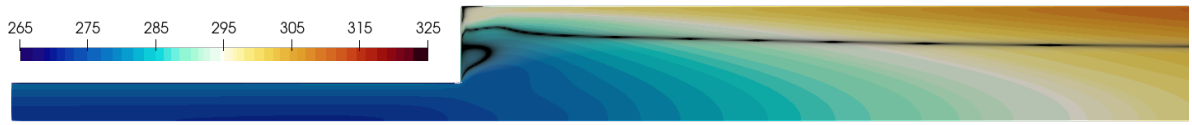

Figure 6: Total temperature (in K) near the inlet and in the cold outlet of the vortex tube for P_{0in}=239 kPa and μ_c=0.6. The black line delimits the flow reversal zone.

temperature profile near the inlet. This term is deemed necessary to predict the reverse static temperature profiles near the inlet.

The different terms in the energy equation were also presented in a dimensionless form. The pressure gradient term was compared to the other energy transfer mechanisms. This analysis demonstrated that the pressure work term is one order of magnitude higher than the heat transfer and the shear work in the radial direction across the flow reversal line. The analysis also highlighted a recirculation zone near the inlet, which is believed to be detrimental to the energy separation process. However, more complex turbulence models are deemed necessary to better predict the magnitude of the pressure gradient from a better prediction of the tangential velocity profile.

NOMENCLATURE

$\bar{\bar{B}}$	velocity tensor	(s^{-1})
c	speed of sound	($m \cdot s^{-1}$)
c_p	specific heat at constant pressure	($J \cdot kg^{-1} \cdot K^{-1}$)
D	diameter	(m)
e	specific internal energy	($J \cdot kg^{-1}$)
Ec	Eckert number	(–)
h	specific enthalpy	($J \cdot kg^{-1}$)
$\bar{\bar{I}}$	identity tensor	(–)
k	turbulence kinetic energy	($m^2 \cdot s^{-2}$)
Ma	Mach number	(–)
P	pressure	(Pa)
r	radius	(m)
R	specific gas constant	($J \cdot kg^{-1} \cdot K^{-1}$)
Re_D	Reynolds number based on the diameter	(–)
S_{kh}	pressure gradient source term	($W \cdot m^{-3}$)
T	temperature	(K)
v	velocity	($m \cdot s^{-1}$)
V	velocity magnitude	($m \cdot s^{-1}$)
y^+	nondimensional wall distance	(–)
γ	specific heat ratio	(–)
ε	rate of dissipation of k	($J \cdot kg^{-1} \cdot s^{-1}$)
λ	thermal conductivity	($W \cdot m^{-1} \cdot K^{-1}$)
μ	dynamic viscosity	($kg \cdot m^{-1} \cdot s^{-1}$)
μ_c	cold mass fraction	(–)
ρ	density	($kg \cdot m^{-3}$)
$\bar{\bar{\tau}}$	shear stress tensor	($kg \cdot m^{-1} \cdot s^{-2}$)
ω	specific dissipation rate	(s^{-1})
ω_a	angular velocity	(s^{-1})

Superscripts

$\vec{}$	vector
”	density-weighted fluctuating velocity
*	nondimensional quantities

Subscripts

0	total condition
c	cold outlet
eff	effective
h	hot outlet
in	inlet
m	molecular
t	turbulent
vt	vortex tube

Abbreviations

2D	two-dimensional
CFD	computational fluid dynamics

REFERENCES

Aljuwayhel, N. F., Nellis, G. F., & Klein, S. A. (2005). Parametric and internal study of the vortex tube using a CFD model. *Int. J. Refrig.*, *28*(3), 442–450.

ANSYS. (2022). *Ansys Fluent theory guide* (2022R1 ed.).

Behera, U., Paul, P. J., Dinesh, K., & Jacob, S. (2008). Numerical investigations on flow behaviour and energy separation in Ranque-Hilsch vortex tube. *Int. J. Heat Mass Transf.*, *51*(25-26), 6077–6089.

Behera, U., Paul, P. J., Kasthurirengan, S., Karunanithi, R., Ram, S. N., Dinesh, K., & Jacob, S. (2005). CFD analysis and experimental investigations towards optimizing the parameters of Ranque-Hilsch vortex tube. *Int. J. Heat Mass Transf.*, *48*(10), 1961–1973.

Bej, N., & Sinhamahapatra, K. P. (2016). Numerical analysis on the heat and work transfer due to shear in a hot cascade Ranque-Hilsch vortex tube. *Int. J. Refrig.*, *68*, 161–176.

Camiré, J. (1995). *Experimental investigation of vortex tube concepts* (Unpublished master's thesis). University of British Columbia, Vancouver, Canada.

Chen, J., Zeng, R., Zhang, W., Qiu, L., & Zhang, X. (2018). Numerical analysis of energy separation in Ranque-Hilsch vortex tube with gaseous hydrogen using real gas model. *Appl. Therm. Eng.*, *140*, 287–294.

Cockerill, T. T. (1998). *Thermodynamics and fluid mechanics of a Ranque-Hilsch vortex tube* (Unpublished master's thesis). University of Cambridge, Cambridge, UK.

Deissler, R. G., & Perlmutter, M. (1960). Analysis of the flow and energy separation in a turbulent vortex. *Int. J. Heat Mass Transf.*, *1*(2-3), 173–191.

Dutta, T., Sinhamahapatra, K. P., & Bandyopadhyay, S. S. (2021). Experimental and numerical investigation of energy separation in counterflow and uniflow vortex tubes. *Int. J. Refrig.*, *123*, 9–22.

Dyck, N., & Straatman, A. (2018). Energy transfer mechanisms in the Ranque-Hilsch vortex tube. In *Proceedings of the Canadian Society for Mechanical Engineering International Congress, Toronto, Canada* (pp. 1–5). CSME-SCGM.

Farouk, T., & Farouk, B. (2007). Large eddy simulations of the flow field and temperature separation in the Ranque-Hilsch vortex tube. *Int. J. Heat Mass Transf.*, *50*(23-24), 4724–4735.

Gao, C. (2005). *Experimental study on the Ranque-Hilsch vortex tube* (Unpublished doctoral dissertation). Technische Universiteit Eindhoven, The Netherlands.

Kaufmann, A. (2022). *The Ranque Hilsch vortex tube demystified: understanding the working principles of the vortex tube*. Springer Nature. (72 p.)

Khait, A. V., Noskov, A. S., Lovtsov, A. V., & Alekhin, V. N. (2014). Semi-empirical turbulence model for numerical simulation of swirled compressible flows observed in Ranque-Hilsch vortex tube. *Int. J. Refrig.*, *48*, 132–141.

Kobiela, B., Younis, B. A., Weigand, B., & Neumann, O. (2018). A computational and experimental study of thermal energy separation by swirl. *Int. J. Heat Mass Transf.*, *124*, 11–19.

Kolmes, E. J., Geyko, V. I., & Fisch, N. J. (2017). Heat pump model for Ranque–Hilsch vortex tubes. *Int. J. Heat Mass Transf.*, *107*, 771 - 777.

Lagrandeur, J., Croquer, S., Poncet, S., & Sorin, M. (2021). A 2D numerical benchmark of an air Ranque-Hilsch vortex tube based on a fractional factorial design. *Int. Commun. Heat Mass Transf.*, *125*, 105310.

Lagrandeur, J., Poncet, S., & Sorin, M. (2019). Review of predictive models for the design of counterflow vortex tubes working with perfect gas. *Int. J. Therm. Sci.*, *142*, 188–204.

Lagrandeur, J., Poncet, S., Sorin, M., & Khennich, M. (2019). Thermodynamic modeling and artificial neural network of air counterflow vortex tubes. *Int. J. Therm. Sci.*, *146*, 106097.

Lamberts, O. (2018). *Compressible Reynolds-averaged Navier-Stokes equations* (Tech. Rep.). Université Catholique de Louvain. (13 p.)

Ouadha, A., Baghdad, M., & Addad, Y. (2013). Effects of variable thermophysical properties on flow and energy separation in a vortex tube. *Int. J. Refrig.*, *36*(8), 2426–2437.

Shtern, V. N., & Borissov, A. A. (2010). Nature of counterflow and circulation in vortex separators. *Phys. Fluids*, *22*(8), 083601.

Skye, H. M., Nellis, G. F., & Klein, S. A. (2006). Comparison of CFD analysis to empirical data in a commercial vortex tube. *Int. J. Refrig.*, *29*(1), 71–80.

Stephan, K., Lin, S., Durst, M., Huang, F., & Seher, D. (1984). A similarity relation for energy separation in a vortex tube. *Int. J. Heat and Mass Transf.*, *27*(6), 911–920.

Tyutyuma, V. D. (2016). Influence of thermal processes on the efficiency of the energy separation in a Ranque vortex tube. *J. Eng. Phys. Thermophys.*, *89*(6), 1505–1513.

Wilcox, D. C. (1998). *Turbulence modeling for CFD* (2nd ed.). La Cañada, CA, USA: DCW industries.

Xue, Y., Arjomandi, M., & Kelso, R. (2010). A critical review of temperature separation in a vortex tube. *Exp. Therm. Fluid Sci.*, *34*(8), 1367 - 1374.

Yusof, M. H. b., Katanoda, H., & Morita, H. (2015). Temperature and pressure measurements at cold exit of counter-flow vortex tube with flow visualization of reversed flow. *J. Therm. Sci.*, *24*(1), 67–72.

ACKNOWLEDGMENT

Authors acknowledge the support of the NSERC chair on industrial energy efficiency established in 2019 at Université de Sherbrooke and funded by Hydro-Québec, Natural Resources Canada and Emerson Commercial and Residential Solutions. All calculations have been performed using the HPC facilities of the Compute Canada network, which is also gratefully acknowledged.